

Complex-band structure: a method to determine the off-resonant electron transport in oligomers

Giorgos Fagas ^{a *}, Agapi Kambili ^a, and Marcus Elstner ^b

^aInstitut für Theoretische Physik, Universität Regensburg
D-93040 Regensburg, Germany

^bTheoretische Physik, Universität Paderborn, D-33098 Paderborn, Germany, and
Abteilung für Molekulare Biophysik, Deutsches Krebsforschungszentrum, D-69120 Heidelberg, Germany

We validate that off-resonant electron transport across *ultra-short* oligomer molecular junctions is characterised by a conductance which decays exponentially with length, and we discuss a method to determine the damping factor via the energy spectrum of a periodic structure as a function of complex wavevector. An exact mapping to the complex wavevector is demonstrated by first-principle-based calculations of: a) the conductance of molecular junctions of phenyl-ethynylene wires covalently bonded to graphitic ribbons as a function of the bridge length, and b) the complex-band structure of poly-phenyl-ethynylene.

1. Introduction

Since the pioneering theoretical proposal of a molecular rectifier by Aviram and Ratner [1], molecular electronics has received considerable attention [2]. A first key experiment [3] investigated the predictions of tunnel theory. It established the exponential decrease of the conductance in Langmuir-Blodgett $[\text{CH}_3(\text{CH}_2)_{N-2}\text{COO}]_2\text{Cd}$ films between Al electrodes versus their thickness for chain lengths $N=18-22$. Most recently, in an effort to illuminate the mechanism of electron transport in relatively short mono-molecular junctions, such length dependence has been reported in experiments with scanning probe microscopy techniques [4,5,6,7], where a small number of molecules contributes to the conductance. Structure dependent factors have been studied by looking at a variety of oligomers, and by systematically varying the contact to the electrodes via the anchor groups or the tip load. In some cases, measured molecules had chain lengths ranging from one up to four monomer units [4,5,6]. All results point to through-bond off-resonant tunnelling transport.

In metal-molecule-metal junctions (MMMs), the molecular electronic states hybridise with the metal wavefunctions giving a finite width in the energy space. If no large charge transfer occurs from/to the molecule, the Fermi energy E_F lies within the (broadened and shifted) highest-occupied- and lowest-unoccupied- molecular-orbital (HOMO-LUMO) energies. Such an alignment poses a potential barrier to traversing electrons accounting for tunnelling. In this regime, there is an analogy of MMMs to metal-insulator (or metal-semiconductor) junctions, and of the molecular-orbital energy broadening to the metal-induced gap states (MIGS) [8,9,10,11].

Such states are induced by matching to the metal side, appear at energies within the band-gap of the insulator (semiconductor), and decay exponentially away from the junction in the non-metal [8]. MIGS are responsible for the overall finite density of states (DOS) within the HOMO-LUMO gap E_g for short molecular wires because of contributions coming from both electrodes [9]. For longer wires, one expects the MIGS to be mainly located near the interfaces on either side of the molecule. By looking at the positional dependence of the local DOS, such behaviour has been observed for Si nanowires between Al electrodes

*Corresponding author:
giorgos.fagas@physik.uni-regensburg.de

[10] and octanedithiols between Au (111) surfaces [11]. In the latter case, a one-to-one correspondence between the local DOS decay parameter and the complex wavevector of wavefunctions in the forbidden energy domain of the corresponding one-dimensional crystal, was found.

Such a property has been conjectured to also hold for the damping factor β of the conductance of oligomer molecular junctions [11,12,13], deep in the tunnelling regime, where $\beta N \gg 1$. The physical meaning of β arises naturally, and the dispersion relation with complex wavevector may be used to define an effective mass of tunnelling electrons [11,13]. However, since most studies assume that $\beta N \gg 1$, the range of validity of such tunnelling characteristics is unclear. In what follows, we elaborate on this and demonstrate that the conductance decays almost always with length in an exponential fashion. We focus on the damping factor of electron transport across oligomers which is the relevant quantifying quantity, readily deducible experimentally. In particular, we establish its connection to the band structure of the corresponding polymer when extended in the complex wavevector plane. Most importantly, this mapping holds even for very short bridges consisting of a handful of monomer units, as in experiments, and for surprisingly small values of the damping factor, providing an indispensable tool for the understanding and prediction of the tunnelling phenomena involved.

2. Electron transport framework

The low-bias and low-temperature electronic response of the MMMs is determined by the elastic scattering of independent electrons with energy E for molecular wires in which electron resident times are small compared to those of molecular vibrations [2]. Electrons see a frozen-nuclei configuration and, in a first approximation, the main contribution derives from equilibrium conditions. Polaronic effects may also be disregarded for molecular bridges of the size we consider [14], whereas, the response is voltage independent [15]. The Landauer conductance g is

$$g(E) = \frac{2e^2}{h} T(E), \quad (1)$$

where the transmission function T denotes the total transition probability from incoming to outgoing states at mutually exclusive electrodes. The temperature constrain is relaxed by comparing the molecular energy scales (\sim eV) to room temperature (\approx 25meV).

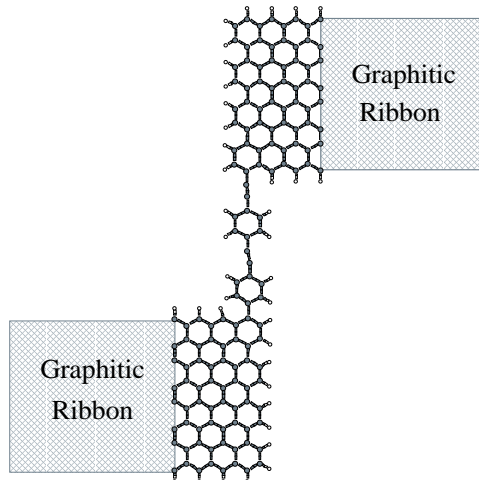


Figure 1. Structure of diphenyl-ethynylene bonded to two graphitic electrodes. Open circles denote hydrogen atoms. See Sec.4 for more details.

For energies far-off the molecular bridge resonant-spectrum and relatively long wires, the transmission function has been studied in both model systems and realistic molecular junctions [12,16,17,18,19]. It shows the characteristic exponential length dependence of a tunnelling process

$$T(E) = T_o(E) e^{-\beta(E)(N-1)}, \quad (2)$$

where N represents the number of monomers that constitute the molecular wire. In Sec.5, we show that Eq.2 is of more general validity.

The pre-exponential factor relates to the molecule/electrode interface; it defines the contact conductance g_o in units of $(2e^2/h)$. In the long oligomer limit, the damping factor β is a property of the bridge, related to its electronic structure. Based on WKB approximation a sim-

ple expression reads

$$\beta(E) = 2\sqrt{\frac{2m}{\hbar^2}E_{g'}}, \quad (3)$$

where $E_{g'}$ equals E_g or $|E - E_{\text{HOMO(LUMO)}}|$. However, this overestimates β [11,13] and calls for an elaborated approach as discussed later.

To investigate the conductance properties of molecular junctions as that of Fig.1, we calculate the transmission function with Green function methods of quantum transport [20] via

$$T(E) = \text{Tr}[\mathbf{\Gamma}_L(E)\mathbf{G}^r(E)\mathbf{\Gamma}_R(E)\mathbf{G}^a(E)]. \quad (4)$$

$\mathbf{G}^{r(a)}$ = $(E\mathbf{S} - \mathbf{H} - \mathbf{\Sigma})^{-1}$ is the retarded (advanced) molecular Green function dressed by a self-energy interaction $\mathbf{\Sigma} = \mathbf{\Sigma}_L + \mathbf{\Sigma}_R$. This follows the Löwdin projection technique and takes into account the coupling to the 'left' (L) and 'right' (R) electrodes. Twice the imaginary part of $\mathbf{\Sigma}_{L(R)}$ defines the spectral width $\mathbf{\Gamma}_{L(R)}$. Since we are interested in the low-voltage regime we use the equilibrium Green function. We have assumed a non-orthogonal basis which introduces the overlap matrix \mathbf{S} , and an algebraic procedure with finite dimensional matrices.

To treat the electronic structure of the oligomer and the electrodes, we employ a linear combination of atomic orbitals approach parameterised by Density Functional Theory (DFT-TB) [21] in the local density approximation (LDA). In DFT-TB, the single-particle electronic Kohn-Sham eigenstates ψ_i of the system are expanded in a non-orthogonal basis set φ_μ for valence electrons located at the ionic positions \mathbf{R}_μ , namely

$$\psi_i(\mathbf{r}) = \sum_{\mu} c_{\mu}^i \varphi_{\mu}(\mathbf{r} - \mathbf{R}_{\mu}). \quad (5)$$

The basis set is computed in terms of Slater-type orbitals in a modified atomic potential that slightly compresses the electron density to take into account that atoms are brought together in a condensed state. With the *Ansatz* of Eq.5 the Kohn-Sham equations for ψ_i are transformed to a set of algebraic equations

$$\sum_{\nu} (H_{\mu\nu} - S_{\mu\nu}E_i)c_{\nu}^i = 0. \quad (6)$$

The tight-binding (TB) approximation assumes superimposing atomic densities when calculating potential contributions [22]. $H_{\mu\nu}$ include only two-centre, distance-dependent, Hamiltonian matrix elements. Eq.6 is of the extended Hückel type but all elements are calculated numerically without empirical parameters. Moreover, the a priori parameterisation of \mathbf{H} and \mathbf{S} provides an efficient scheme for calculating the Green functions.

3. Complex-band structure

Assuming that interfacial effects are not dominant, any evanescent states in an underlying periodic system are understood as bulk Bloch states with a k vector with an imaginary component, i.e., $k = q - i\kappa$. These states are quantified by the complex-band structure, the extension of the electronic band structure to include complex Bloch vectors. In band structure calculations, real k in the first Brillouin zone are given as input to solve the energy eigenvalue problem. For the complex-band structure, the inverse problem is defined. All k vectors associated with a real energy E are sought, which are in general complex. The analytic properties of the energy spectrum of crystals as function of a complex variable have been initially studied by Kohn [23].

In any case, Eq.6 in a periodic potential is solved, which within our TB approximation reads

$$\begin{aligned} (\mathbf{H}_{m,m} + \mathbf{H}_{m,m+1}e^{ika} + \mathbf{H}_{m-1,m}e^{-ika})\phi_k^E &= \\ E_k(\mathbf{S}_{m,m} + \mathbf{S}_{m,m+1}e^{ika} + \mathbf{S}_{m-1,m}e^{-ika})\phi_k^E. \end{aligned} \quad (7)$$

The matrices $\mathbf{H}_{i,j}$ and $\mathbf{S}_{i,j}$ contain the Hamiltonian and overlap elements, respectively, between the i th and j th monomer units; a is the lattice constant. Furthermore, we employ a useful algorithm based on transforming Eq.7 to a generalised eigenvalue problem for $\lambda \equiv e^{ika}$, yielding

$$\begin{aligned} \left(\begin{array}{cc} \mathbf{H}_{m,m} - E\mathbf{S}_{m,m} & \mathbf{H}_{m-1,m} - E\mathbf{S}_{m-1,m} \\ \mathbf{I} & \mathbf{0} \end{array} \right) \tilde{\phi}_{\lambda} \\ = \lambda \left(\begin{array}{cc} -(\mathbf{H}_{m,m+1} - E\mathbf{S}_{m,m+1}) & \mathbf{0} \\ \mathbf{0} & \mathbf{I} \end{array} \right) \tilde{\phi}_{\lambda}. \end{aligned} \quad (8)$$

The procedure resembles finding the eigenvalues

of the transfer matrix in a non-orthogonal localised basis set but it overcomes problems arising from possible singular matrices. This formal similarity also justifies a relation of β to the complex wavevector. We solve numerically Eq.8 for any real E and classify its eigenvalues. For $|\lambda| = 1$, k is real; otherwise k is complex and describes exponentially decaying or growing solutions, which are of particular interest in the tunnelling regime.

4. Prototype system

The molecular junctions under investigation consist of oligo-phenyl-ethynylene (OPE) wires of small varying length connected to two graphene electrodes in a ribbon shape. Before calculating the conductance of systems as that depicted in Fig.1, all the formed molecular junctions are optimised. More precisely, the non-shaded area is dispatched and the consequent edges are replaced by single hydrogens. To simulate the bulk electrodes, a constrained atomic relaxation is performed. Graphene atoms away from the OPE/ribbon interfacial bond by approximately $3 \times$ hexagonal lattice constant remain immovable. The shaded-area represents infinite graphitic ribbons whose structure is assumed not to differ from that of perfect graphene with H saturated edges. As an input for C-H and single/triple C-C bonds in the graphitic part and OPE, we use standard literature values. For the interfacial contact, we take a single C-C bond with 1.39\AA .

The choice of ribbons (width as shown in Fig.1) of single-layered graphite is guided by recent experimental reports [24]. In those, self-assembled-monolayers of conjugated molecules were deposited on a graphitic substrate. The molecular phenyl rings form a covalent bond to the carbon electrode in a similar fashion to that of Fig.1, which ensures a low energy barrier at the interface. Our junctions is a first effort to model nanographite materials and may be considered as an idealisation with the following approximations: a) the graphite material is well-ordered, b) the weak inter-plane interactions in graphite are insignificant, and c) there is weak inter-molecular interaction. These assumptions must be studied in detail separately, which is beyond our present

scope. Later we discuss the validity of our results when other metals are considered as electrodes. Our motivation also stems from abiding interest in carbon-based nanojunctions [25,26].

5. Results - Discussion

We have calculated the conductance spectra for OPE wires consisting of up to five monomer units in a large energy window spanning the valence and conduction bands of poly-phenyl-ethynylene (PPE), using the formulation of Sec.2. In Fig.2, we plot for selected energies the logarithm of the transmission function for OPE molecular junctions of increasing length, represented by the number of monomer units N . The inset shows the local density of states at the carbon atom of the graphitic electrode which bonds to the oligomer.

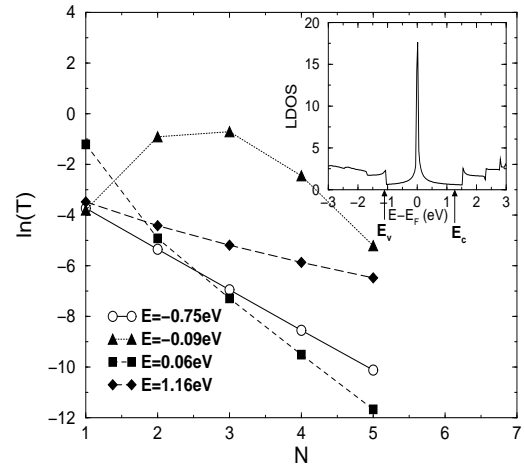


Figure 2. Logarithm of the transmission function $T(E)$ as function of the OPE length $N\alpha$, for various energies E . All energies are measured from E_F and lie in the band-gap of PPE. The inset shows the local DOS at the contact carbon atom of the graphitic electrode to the oligomer.

There are two types of curves evident in Fig.2. One type, e.g., at $E = -0.75\text{eV}$ and 1.16eV , clearly indicates an exponential decrease of $T(E)$ with length, from practically $N = 1$. This behaviour is robust for almost all energies inside the gap formed by the renormalised HOMO-

LUMO energies of the embedded OPE. This gap is slightly larger than the band-gap of PPE, allowing for the tunnelling behaviour. The other type of curve is approximated by Eq.2 after a minimum length; for $E = 0.06\text{eV}$ at $N \approx 2$ and for $E = -0.09\text{eV}$ at $N \approx 3$. The latter data show an anomalous length dependence with an initial increase of the conductance for $N < 3$. Such behaviour relates to unconventional MIGS [26]. These provide a way of molecular doping in short junctions that opens an additional resonant-tunnelling conduction channel.

Unconventional MIGS are manifested when there is a large local DOS on the metal side. Indeed, the local DOS (inset of Fig.2) at the electrode interfacial contact of our molecular junction exhibits (van Hove) singularities. A most pronounced peak lies within the gap of PPE at the Fermi level of the system. This corresponds to a state located predominantly at the zigzag edges of the graphene ribbon [27] and is responsible for the main departures of $T(E)$ from Eq.2. Nevertheless, the tunnel effect is still observed for quite small chain lengths and energies not in the immediate vicinity of local DOS peaks ($\sim 10\text{meV}$), enabling the extraction of β . This is a striking result since it extends the applicability of Eq.2 to ultra-short oligomer bridges and to a wide energy spectrum not far-off to that responsible for resonant-tunnelling.

We now turn our attention to the electronic structure of perfect PPE. Its complete band structure is calculated as described in Sec.3 via Eq.7 and 8, and is shown in Fig.3. The right panel corresponds to the conventional band structure. The spectrum of the imaginary part of complex k solutions, which come in conjugate pairs ($\pm\kappa$), is plotted in the left panel. The complex-band structure shows the typical excursions which connect real bands between local extrema.

An accurate complex-band structure calculation is necessary for a comprehensive quantitative account of the MIGS [28]. We have made additional calculations for alkane chains, graphene, and poly-para-phenylene (PPP). In all cases, our calculated band structures both in the real axis and in the complex plane, are in good agreement with those reported for either minimal or plane

wave basis sets within DFT in the LDA [11,29,30]. Moreover, as described in Sec.3, MIGS are associated with the complex k vectors for real energies and are exponentially decaying. Hence, we anticipate that states with the smallest $|\kappa|$ are dominant. Namely, of most importance for quantifying the damping factor in Eq.2 is the, so-called, real-line connecting the top of the valence and bottom of the conduction bands, which occur at the border of the Brillouin zone $k = \pi/\alpha$. This line joins the energies $E_v = -1.12\text{eV}$ and $E_c = 1.25\text{eV}$, and is reproduced quite accurately within DFT-TB.

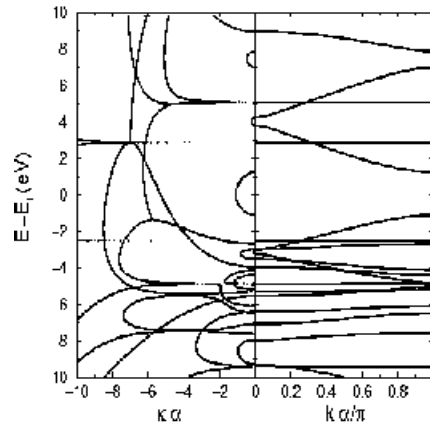


Figure 3. Complex- and real- band structure of PPE in left and right panel, respectively.

In Fig.4, we isolate the positive branch of the E_c to E_v real-line and plot it on a larger scale. Together we plot the half of the damping factor β , which is numerically obtained by a least-squares fit to determine the slope of the lines in Fig.2. For energies where $T(E)$ exhibits a non-monotonic length dependence, we have used only data for $N > 2$. The agreement is evidently remarkable for the entire energy spectrum, even at very small values of the tunnel decay parameter.

There are hardly deviations from the relation $\beta(E) = 2|\kappa(E)|\alpha$. κ denotes that value of real-lines at E with the largest imaginary part in the renormalised HOMO-LUMO gap of the oligomer. Small irregularities appear only at those energies that the graphitic ribbons have a large local DOS. This marks the specific system and may not ap-

pear if strong disorder in graphene washes out the singularities. Since our results point to the intrinsic character of the damping factor for almost any $\beta(E)N$, we expect an even better agreement in the usual case of Al or Au electrodes. On the one hand, such broad-band metals usually exhibit seamless local DOS. On the other, larger interfacial barriers are formed in comparison to that of the C-C bond, due to the groups anchoring the metal. Small departures similar to those caused by the unconventional MIGS may occur if the anchor groups have localised states within the spanned energy window [11,29].

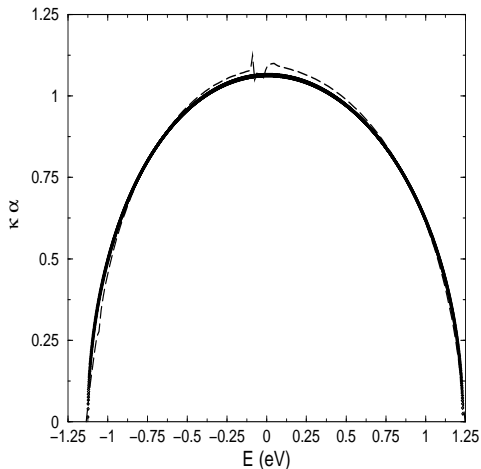


Figure 4. The E_c to E_v real-line from Fig.3 (solid) and the half of the damping factor as extracted from the slope of transmission function lines (see Fig.2) for all energies (dashed).

Our results generally apply to oligomer bridges between metals in the off-resonant regime. They explain qualitatively the microscopic transport mechanism in experiments of ultra-short oligomer molecular junctions [4,5,6], and results obtained with non-equilibrium Green functions [31]. For tunnelling, an analysis [15] similar to the Simmons model [32], but including the spatial discreteness at these length-scales, may be used to derive current-voltage characteristics. E_F is estimated by comparison of the extracted damping factor to the complex wavevector [7].

Conversely, E_F is roughly located at the maximum of the E_c to E_v real-line for metal-insulator (metal-semiconductor) junctions [11], which approximately holds for the nanojunctions we studied. Using this argument, we have calculated the damping factors for other polymers from the complex wavevector at the middle of their band-gap. For PPP we found $\beta(E=0) = 1.8$, which is in quantitative agreement with the reported experimental [5,6] and theoretical [31] values in MMMs of oligo-para-phenyl chains (OPP) up to four units between Au electrodes. However, one should take into account the possibility of non-planar intramolecular phenyl-ring alignment in OPP. We shall report on such effects in forthcoming studies [33] and compare with other calculations of the complex-band structure for twisted phenyl-ring geometries [29].

6. Concluding remarks

We demonstrated that no tunnel-barrier collapse occurs even for *ultra-short* oligomer molecular junctions, and for virtually *all energies* within the gap of the corresponding polymer, $E_c - E_v$. Contrary to expectations, there exists a unique damping factor $\beta(E)$, even though $\beta(E)N \gg 1$ is not always valid. This is traced back to the larger value, in comparison to the band-gap $E_c - E_v$, of the renormalised HOMO-LUMO gap of the oligomers in the junction.

Moreover, we indicated the importance of calculating, and the need to understand and find ways to engineer, the complex-band structure of molecular wires. Our results establish that the damping factor $\beta(E)$ can be almost exactly mapped to the complex wavevector for all energies within $E_c - E_v$. This substantiates that the complex-band structure provides a prolific method to determine the most crucial property of off-resonant electron transport across oligomer molecular junctions without performing a transport calculation. Improved independent first-principle methods may be used to increase the accuracy in evaluating β .

Our calculations on phenyl-ethynyl chains show that a single complex wavevector is adequate to explain the tunnelling regime but it cannot be ex-

cluded that a superposition of contributions from few close-by complex- k may be needed to understand electron transport across other oligomers. Although there are strong indications that our results apply in many cases, further investigations are clearly necessary to identify the typical behaviour. In favour of the former are independent calculations on complex-band structures of various molecular wires, the rapid convergence of tunnelling decay constants of short oligomers to the long wire limit (see also [34,35]), and simple qualitative arguments on the sensitivity of transport observables to small deviations in $|\kappa|$ due to tunnelling.

The derived connection to the metal-induced gap states fortifies the analysis of the conductance properties of molecular junctions by using concepts developed in the theory of metal-insulator (metal-semiconductor) junctions. On the other hand, the tunnel properties of oligomers are of special relevance to molecular electronic devices and new circuit-designs. Finally, we note the conceptual similarity between electron transport in metal-molecule-metal junctions and the fundamental chemical process of molecular electron transfer. Indeed, a formal analogy in a simple model relates the non-adiabatic electron transfer rate k_{DA} in a donor-bridge-acceptor system to the Landauer conductance [2]. The expression Eq.2 is reminiscent of the superexchange mechanism, and β coincides with McConnell's result [34,35].

Acknowledgements

AK is thankful to the Alexander von Humboldt Stiftung. GF was supported by the DFG Graduiertenkolleg Nichtlinearität und Nichtgleichgewicht in kondensierter Materie. The authors thank Klaus Richter for his critical comments and Rafael Gutierrez for discussing the manuscript.

REFERENCES

1. A. Aviram and M.A. Ratner, Chem. Phys. Lett. 29 (1974) 277.
2. A. Nitzan and M.A. Ratner, Science 300 (2003) 1384.
3. B. Mann and H. Kuhn, J. Appl. Phys. 42 (1971) 4398.
4. H. Sakaguchi, A. Hirai, F. Iwata *et al*, Appl. Phys. Lett. 79 (2001) 3708.
5. D.J. Wold, R. Haag, M.A. Rampi *et al*, J. Phys. Chem. B 106 (2002) 2813.
6. T. Ishida, W. Mizutani, Y. Aya *et al*, J. Phys. Chem. B 106 (2002) 5886.
7. X.D. Cui, A. Primak, X. Zarate *et al*, J. Phys. Chem. B 106 (2002) 8609.
8. V. Heine, Phys. Rev. 138 (1965) A1689.
9. N.D. Lang and Ph. Avouris, Phys. Rev. B 64 (2001) 125323.
10. U. Landman, R.N. Barnett, A.G. Schebakov *et al*, Phys. Rev. Lett. 85 (2000) 1958.
11. J.K. Tomfohr and O.F. Sankey, Phys. Rev. B 65 (2002) 245105.
12. A. Onipko, Y. Klymenko, L. Malysheva, S. Stafström, Solid State Comm. 108 (1998) 555.
13. C. Joachim and M. Magoga, Chem. Phys. 281 (2002) 347.
14. H. Ness, S.A. Shevlin, and A.J. Fisher, Phys. Rev. B 63 (2001) 125422.
15. V. Mujica and M.A. Ratner, Chem. Phys. 264 (2002) 365.
16. V. Mujica, M. Kemp, and M.A. Ratner, J. Chem. Phys. 101 (1994) 6856.
17. M. Magoga and C. Joachim, Phys. Rev. B 57 (1998) 1820.
18. L.E. Hall, J.R. Reimers, N.S. Hush, and K. Silverbrook, J. Chem. Phys. 112 (2000) 1510.
19. C. Joachim and J.F. Vinuesa, Europhys. Lett. 33 (1996) 635.
20. S. Datta, Electronic Transport in Mesoscopic Systems, Cambridge University Press, Cambridge (1995).
21. D. Porezag, Th. Frauenheim, Th. Köhler *et al*, Phys. Rev. B 51 (1995) 12947.
22. M. Elstner, D. Porezag, G. Jungnickel *et al*, Phys. Rev. B 58 (1998) 7260.
23. W. Kohn, Phys. Rev. 115 (1959) 809.
24. F. Anariba and R.L. McCreery, J. Phys. Chem. B 106. (2002) 10355
25. G. Fagas, G. Cuniberti, and K. Richter, Phys. Rev. B 63 (2001) 045416.
26. R. Gutierrez, G. Fagas, K. Richter *et al*, Europhys. Lett. 62 (2003) 90.
27. K. Nakada, M. Fujita, G. Dresselhaus, M.S.

- Dresselhaus, Phys. Rev. B 54 (1996) 17954.
28. F. Picaud, A. Smogunov, A. Dal Corso *et al*, J. Phys.: Condens. Matter 15 (2003) 3731.
 29. J.K. Tomfohr and O.F. Sankey, Phys. Stat. Sol. (b) 233 (2002), 59.
 30. T. Kawai, Y. Miyamoto, O. Sugino, Y. Koga, Phys. Rev. B 62 (2000) R16349.
 31. C. Kaun, B. Larade, and H. Guo, Phys. Rev. B 67 (2003) 121411.
 32. J.G. Simmons, J. Appl. Phys. 34 (1963) 1793.
 33. G. Fagas and A. Kambili, *preprint*.
 34. H.M. McConnell, J. Chem. Phys. 35 (1961) 508.
 35. J.R. Reimers and N.S. Hush, J. Photochem. Photobiol. A 82 (1994) 31.